Materials Today Sustainability 18 (2022) 100134

Contents lists available at ScienceDirect

Materials Today Sustainability

journal homepage: https://www.journals.elsevier.com/materials-today-sustainability

Cationic graphene-based polymer composite modified with chromium-based metal-organic framework [GP/MIL-53(Cr)] for the degradation of 2,4-dichlorophenol in aqueous solution

B.A. Oni [a, b, *], S.E. Sanni [b]

[a] Chemical Engineering Department, China University of Petroleum, Changping District, Beijing, China
[b] Chemical Engineering Department, Covenant University, km 10 Idiroko Road, Ota, Nigeria

ARTICLE INFO

Article history:
Received 8 February 2022
Received in revised form
23 March 2022
Accepted 25 March 2022
Available online 12 April 2022

Keywords:
Adsorption
Graphene
2,4 dichlorophenol
Wastewater
Chromium-based metal-organic framework

ABSTRACT

Owing to its remarkable water stability, chromium-based metal-organic framework (MIL-53(Cr) has the capacity to remove 2,4-dichlorophenol (2,4-DCP) from aqueous solutions, but the weak adsorptive capacity of the adsorbent limits its utilization. In this work, cationic graphene-based polymer composite (GP) was successfully synthesized with (MIL-53(Cr)) [GP/MIL-53(Cr)] through one-step solvothermal technique and characterized with XRD, SEM, BET, XPS, TEM, and FTIR. Adsorbent dose, pH, initial concentration, and contact time were enhanced to improve the performance of GP/MIL-53(Cr). GP/MIL-53(Cr) displayed a marginal adsorptive performance relative to MIL-53(Cr) and GP. The adsorption of 2,4-DCP mainly depends on the nature of MIL-53(Cr) and the electrostatic attractions of the functional groups on GP surface. Due to the high magnetic properties of GP/MIL-53(Cr), effective solid−liquid separation can be easily achieved. The adsorbate mineralization process stabilizes at 200 min. The pseudo-second-order model adequately fits the adsorption kinetic data, while the Freundlich and Langmuir models gave a good fit with the equilibrium data. The maximum adsorptive capacity of the adsorbents for the adsorbate as calculated from the Langmuir isotherm are 64.9 (GP), 28.2 MIL-53(Cr), and 98.4 mg/g (GP/MIL-53(Cr). The thermodynamic studies revealed that the adsorption process is spontaneous, feasible, and endothermic. Additionally, the excellent performance of GP/MIL-53(Cr) shows that the adsorbent has potential application in treating wastewater.

1. Introduction

Water is an incredibly valuable resource that must be protected and conserved. Being an important resource for the prevailing fauna and flora, it is important to treat wastewater using relatively cheap and very efficient techniques for use in agriculture and other purposes. The discharge of wastewater from several domestic and industrial activities releases toxic organic (dyes, PAHs, etc.) and inorganic (heavy metal ions) substances, resulting in environmental pollution in the ecosystem [5,10,11,22].

Chlorophenols are waste materials generated during the chemical processing of paints, insecticides, wood preservation, paper production, and herbicides [12]. Low quantities of chlorinated phenols are produced when natural waters are chlorinated for disinfection, especially 2,4-dichlorophenol (2,4-DCP), which is quite prevalent and has been recognized as a key contaminant to be monitored in the marine environment [26]. 2,4-DCP are weak acids that are resistant to biodegradation in general. 2,4-DCP must be degraded before being discharged into waterbodies in order to avoid harmful biomagnification effects on aquatic flora and animals [1]. When 2,4-DCP is present in waterbodies, complex issues such as bad odor and taste in drinking water, as well as the obstruction of routine microbial population activities in wastewater treatment plants may arise [29]. In humans, prolonged exposure to high concentrations of phenol causes severe insomnia, headache, loss of appetite, fast weariness, and malnutrition [13]. The concentration of chlorophenol as low as 0.1 mgL^{-1} can cause hazardous consequences in drinking water [30].

Catalytic hydro de-chlorination, adsorption, Fenton-oxidation/photo-oxidation, volatilization, sono-chemical and electro-chemical degradation, bioremediation (at minimal concentration), and biodegradation are some of the technological advances that

* Corresponding author.
E-mail address: babalola.oni@covenantuniversity.edu.ng (B.A. Oni).

https://doi.org/10.1016/j.mtsust.2022.100134
2589-2347/

could be used to remove these chlorophenolic compounds from wastewater [5,22,26]. Adsorption is one practical technologies for removing cholophenol from chlorophenol-containing effluents.

Most adsorbents, such as polymeric adsorbents, peat, activated carbon, bentonite, and fly ash, have been studied for eliminating chlorophenols from wastewater, which have proven to have relatively low performance in terms of their adsorptive capacities [2,28]. Traditional adsorbents (such as biomass, activated clay minerals, polymeric materials, agricultural waste, zeolite, and so on) have exhibited variable adsorptive capacities towards target pollutants [1].

The mixture of polymer and nanomaterial (such as graphene) is very attractive because it allows new electronic properties to be introduced via electronic interaction and morphological modification that exist between the components [9]. Significant changes in composite qualities can be obtained; however, it depends on the nature of the components employed and the technique of preparation [3]. Various approaches, such as electrochemical encapsulation coating of inorganic polymers, colloidal dispersions, and in situ polymerization with nanoparticles, have been used to produce nanocomposites of conducting polymers, which have provided new pathways for material synthesis [13,26].

Recently, few attentions have been given to the graphene-based polymer composite due to its mechanical, physical, and chemical features [32]. Its enhanced active sites, high surface area, large delocalized π-electron systems, high water solubility, and O_2 containing surface functionalities possess high electrical, good chemical stability, and thermal performance, making it suitable as an adsorbent for wastewater treatment [21]. Reports have shown that graphene-based polymer composite has a high activity/efficiency during wastewater treatment for the removal of heavy metals [3,16,25]. For example, it has been employed for the degradation of potentially toxic heavy metals, ionic dyes, natural organic matter (NOM), 1-butanol dehydration, etc., [16], for instance, the development of graphene oxide/polyacrylamide (GO/PAM composite hydrogels for wastewater treatment using GO as a 2D macromolecule has been reported. The result showed that the mechanical features of GO/PAM hydrogels improved wastewater treatment considerably. GO has a promising applicability in the breakdown of chlorophenols as a result of oxygen-containing functional groups and large surface area.

To date, attention has been given to the use of GO-based composites and polymer/GO [4,8,22,23]. As a result, GO and its modified variants have received a lot of consideration as potential adsorbents for removing heavy metals, pharmaceutical residues, and organic dyes [25]. Notwithstanding, their individual applications are somewhat limited due to the difficulties associated with regenerating the spent adsorbents in an adsorption process. In addition, there are some limitations associated with graphene-based adsorbents when used for chlorophenol removal from an aqueous solution, and these includes a highly polar surface which is indicative of low adsorption, whereby the O_2 groups on the cationic graphene-based polymer adsorb water clusters, thus reducing the adsorption sites [27]. Therefore, there is a need to overcome these limitations that will ease the separation of adsorbate, enhance stronger π-π interactions, hydrophobic interactions, and H-bonding between 2, 4-DCP and the adsorbent, improve the adsorptive capacities, chemical stability, electrical and thermal performances of the adsorbent, thus providing additional sites for adsorption, hence, the introduction of chromium-based metal-organic framework adsorbents.

The water resistance of MIL-53(Cr), as a typical MOF material with a 'breathing effect,' is believed to be superior to other MOFs, which offers the necessary conditions for MIL-53 to be used in liquid phase adsorption. MIL-53(Cr) possesses good water stability and eases separation after adsorption, which makes it more suitable for adsorption in aqueous solutions [23,25]. Several authors have demonstrated the use of (MOFs)MIL-100(Fe)/(GO) [14], (MOFs-HKUST-1/GO [33], Mn-doped UiO-66 MOF/GO, [6] etc., for the removal of contaminants from aqueous solution and their results showed marginal and excellent improvements.

In this article, the authors tried to combine cationic graphene-based polymer composite modified with MIL-53(Cr) for the degradation of 2,4-DCP. To the best of the authors knowledge, no works on this have been carried out. A batch adsorption technique was used to evaluate the adsorbent's efficacy in removing 2,4-DCP. In addition, the isotherms and kinetics of the adsorbent were evaluated, including the adsorbent's recyclability.

2. Materials and method

2.1. Materials

The reagents are ethanol (99.5%), (Cr(NO3)3·9H2O), terephthalic acid (BDC), hydrofluoric acid (HF), and N-dimethylformamide (DMF), which were all purchased from J.T Baker, USA. All chemicals used were of analytical grade without further purification.

Natural graphite was obtained from the Nigeria Ministry of solid minerals, Abuja, Nigeria. Methyl methacrylate (MMA) was purchased from Sinopharm Chemicals and further purified by distillation at reduced-pressure condition prior to use. MAE-TAC, in the form of an aqueous solution (77 wt.%) and 2,2-azobis (2-amidinopropane) dihydrochloride (AIBA) was manufactured by Sigma Aldrich, USA.

2.2. MIL-53(Cr) synthesis

Terephthalic acid (PTA) and $Cr(NO_3)_3 \cdot 9H_2O$ were dissolved in deionized water, with molar ratio Cr: PTA: water = 1.0:1.0:300. After being sonicated for 1 h, 1 mL of 50% HF solution was added dropwise to the solution so as to attain a pH >1, and then sonication continued for the next 1 h. The prepared solution was introduced in a 250 mL hydrothermal kettle and kept in an oven at 200 °C for 72 h. Furthermore, the prepared solution was centrifuged for (six) 6 min at 6000 rpm so as to obtain the precipitate. The precipitate obtained was later washed with N-dimethylformamide and ethanol simultaneously. After washing, the precipitated solid was dried in a vacuum at 120 °C for 24 h, and further calcined at 250 °C in a muffle furnace for 6 h.

2.3. Emulsion polymerization

An emulsion polymerization experiment was conducted in a four-neck round bottom flask. A total of 30 g MMA, 300 mL distilled water, 0.5 g methacryloyloxyethyl trimethyl ammonium chloride (MAE-TAC), and 0.02 g/mL aqueous solution of AIBA was added into the reactor. Polymerization was carried out at 80 °C under N_2 atmosphere. After 5 h, the polymerized emulsion was allowed to cool at 28 °C.

2.4. The synthesis of GO

The synthesized GO was sourced from natural graphite flakes that have been purified following the modified Hummers method [7,15]. A total of 200 mL conc. sulfuric acid was introduced into a 1000 mL flask containing 10 g graphite powder and 4.5 g $NaNO_3$ at 28 °C. The mixture was allowed to cool to 0 °C in an ice bath. Then, 50 g of $KMnO_4$ in solid form (40 g) was gently added (10 g/20 min) to the mixture and stirred using a magnetic stirrer for 24 h 2.5 wt.%, and 400 mL of diluted H_2SO_4 were further added in a dropwise manner into the viscous mixture for 30 min, meanwhile, string continued for the next 1 h. In order to prevent the splashing of the

liquid, a known concentration of H_2O_2 (35 mL, 30 wt.% in water from Sigma Aldrich) was gently added into the mixture for 2 h.

An aqueous solution of GO which is brownish in color was produced after purifying it with a mixture in volume ratio (H_2O: H_2O_2:H_2SO_4; 1.0:0.230:0.260) ten times, followed by two other times. After centrifugation, the supernatant of the solution containing GO was removed; thereafter, the GO powder was obtained at room temperature after vacuum-assisted drying for 24 h.

2.5. Synthesis of polymethyl methacrylate/graphene oxide and polymethyl methacrylate/graphene composites

The GO sheets were treated following Hummers method [24]. The treated GO sheets were filtered, washed, and dried in other to obtain the powdered sheets. The prepared sheets in form of aqueous solution (1 mg/mL) were mechanically stirred and ultrasonicated for 10 min. The obtained solution was added dropwise into the emulsion while stirring. A total of 3.0 wt.% of GO relative to poly (methyl methacrylate) was added to poly (methyl methacrylate) emulsions, and the mixtures was stirred for 2 h at 28 °C, before being centrifuged, washed with distilled water, and dried in an oven under vacuum condition at 110 °C.

The polymethyl methacrylate (PMMA)-graphene composite emulsion (100 mL) was reduced by 2 mL hydrazine, when the mixture was heated to 70 °C for 6 h while constantly stirring. The poly (methyl methacrylate)-graphene composites were obtained in form of powder as illustrated in (Fig. 1).

2.6. MIL-Cr (53)/cationic graphene-based polymer composite preparation

MIL-Cr (53)/cationic graphene-based polymer composite (GP) was synthesized following the solvothermal technique. Cr(NO3)3•9H2O (0.98 g), H_2 BDC (1.2 g), and GP (0.1 g) were introduced in 60 mL (dimethylformamide) DMF and placed in a round bottom flask having a condenser and a magnetic stirrer heated at 130 °C for 24 h under air. The product which was synthesized was obtained after filtration and cooling, and was later placed in an oven for 24 h and maintained at 180 °C so as to eliminate any trapped molecules in the pores.

The sample was characterized using the scanning electron microscopy (SEM) XEI Finton 2000 (USA), transmission electron microscopy (TEM) (Techni G2F20S-TWIN (USA). Others include X-ray photoelectron spectrum (XPS) (DLD AXI-ULTRA, France), Fourier transform infrared (FT-IR) Nicolet 5700 (Thermo Electron, America), X-ray diffraction (XRD) AXSD8 Advance (UK), and a graphite monochromator and UV−vis spectra HITACHIU-4100. The scan rate for each measurement was 200 nm min^{-1}. Brunauer−Emmette−-Teller (BET) nitrogen (N_2) adsorption Micromeritics ASAP 2010 instrument was used to determine the surface area of the composites as well as their pore size distributions.

2.7. Adsorption procedure

All the reagents used are of analytical grade. A total of 100 mg/L concentration of 2,4-DCP in distilled water was prepared in terms of weight by weight (w/w). The adsorption tests were conducted in 250 mL Erlenmeyer flask at 28 °C. The effect of adsorbate solution pH was first analyzed, whereby the adsorbate pH was adjusted between 0.0 and 10.0 with caustic soda or hydrochloric acid solutions. Then, an adsorbate solution containing 100 mL (100 mg/L) and 0.50 g adsorbent was introduced into the flask and stirred at 120 rpm for 6 h. After 1 h of agitating the mixture, a syringe was used to collect the sample and treated for analysis. Solution samples were obtained using a syringe after careful agitation. Secondly, the effect of initial adsorbate concentration of 2,4-DCP was studied at 0.5, 5.0, 50.0, and 100.0 mg/L. Furthermore, other properties were analyzed such as contact time and adsorbent dosage. The adsorbent doses were between 0.0 and 500 mg/L, respectively, with adsorbate solution of 100 mg/L was agitated for 6 h at 150 rpm. Solution samples were obtained at 0, 10.0, 20.0, 30.0, 60.0, 90.0, 120.0 min, respectively. All experiments were conducted in triplicates by taking the average values.

2.8. Adsorption kinetics

Experimentation of the kinetic studies gives useful information of the sample analyzed. The pseudo-first-order and pseudo-second-order kinetic models mimicked the mechanism and the rate of the adsorption of the adsorbate on the adsorbent. Table 1 presents the isotherms, thermodynamic behavior, and kinetic model equations for the adsorption of 2,4-DCP.

2.9. Thermodynamics and adsorption isotherm of 2,4-dichlorophenol

Different adsorption isotherms were tried for 0 to 100 mg/L concentration of the adsorbate for 2 h at 28 °C (room temperature). The Freundlich and Langmuir models the most suitable isotherms mimicked the experimentatal data (Table 1). Thermodynamic properties were also measured in the course of the experiment, they include entropy (ΔS^0), enthalpy (ΔH^0), and the Gibbs free energy (ΔG^0) (Table 1).

3. Results and discussion

3.1. Adsorbent characterization

3.1.1. Scanning electron microscopy analysis

The SEM image of the adsorbents are illustrated in Fig. 2. The GO exhibits some pores on the surface, which are rough compared to those of the MOF (MIL-53(Cr)), and this may be due to the hybridization of PMMA polymer matrices with conducting graphene and polymer derivatives alongside the interactions that exist between the mechanical properties and electrical conductivity (σ). Thus, the mechanical properties of the blends of GO-based PMMA admixed with the MOF were enhanced. It can be seen that the blended adsorbent showed a highly porous structure compared to the unblended adsorbent, thus inducing better properties. The surface modification of the polymer-based graphene helps to generate good bonding between the adsorbents, thus improving

Fig. 1. Production/synthesis of GP/(MIL-53(Cr).

Table 1
Isotherms, thermodynamic, and kinetic models' equation for the adsorption of 2,4-dichlorophenol.

Model	Equation
Langmuir isotherms	$q_e = \frac{q_m K_L C_e}{1 + K_L C_e}$
Freundlich isotherms	$q_e = K_F C_e^{\frac{1}{n}}$
Pseudo-first-order	$In(q_e - q_t) = In\, q_e - \frac{k_1 t}{In\ 10}$
	$q_t = q_{e,\,exp} - \frac{q_{e.exp}}{e^{k_1 t}}$
Pseudo-second-order	$\frac{t}{q_t} = \frac{1}{k_2 q_e^2} + \frac{t}{q_e}$
	$q_t + \frac{t.k_2 q_{e.exp}^2}{1 + t.q_e.k_2}$
Adsorption thermodynamics	$\Delta G = -RT \times In\, k_c$
	$\Delta G^0 = \Delta H^0 - T\Delta S^0\partial$

the efficiency of the adsorbents as well as their multifunctional properties. The cationic GP composite was seen as a wrinkly layered structure, whereas MIL-53(Cr) displays a well-defined octahedral crystal alongside the presence of small uneven particles. The MIL-53(Cr) is haphazardly distributed on the composite surface (GP) sheets, as indicated in the **GP**/MIL-53(Cr).

3.1.2. TEM analysis

The TEM images of the adsorbents further show that the GP/MIL-53(Cr) has a more porous structure compared to modified cationic graphene-based polymer composite and the MOF (MIL-53(Cr) (Fig. 3). It also suggests that GP/MIL-53(Cr) possesses good stability. This visualized morphological variation corroborates the observations of the SEM images, which also suggest that the reduced Cr is evenly distributed on the internal surface of the graphene-based polymer composite. After the adsorbent was contacted with 2,4-DCP, the layered structures were still obvious. The dispersed MIL-53(Cr) in the graphene-based polymer composite can be attributed to the unique GO polymer composite layered structure. During composite formation, the metallic ions from the precursor are evenly distributed on the surface of the graphene composite, specifically at the negative charged sites. The composite mineral which acts as a template, controls the nucleation of the MOF clusters produced as a result of the Cr^{2+} reduction and impedes the particles growth, thereby preventing the **GP**/MIL-53(Cr) from aggregating. Thus, the unique structure may perhaps also make **GP**/MIL-53(Cr) to become highly dispersed in the suspension. Hence, the **GP**/MIL-53(Cr) suspension is stable in water, and the stabilizing effect of **GP**/MIL-53(Cr) as an active dispersant is anticipated.

3.1.3. Fourier transformed infra-red (FT-IR)/Raman spectra of the adsorbents

The FT-IR spectra of A, B, and C are as shown in Fig. 4a. The C=O bonds of (−CHO) in the GP/MIL-53(Cr) adsorbent were detected as an absorption band at 1690 cm^{-1}. The occurrence of $-NH_2$ in the stretching band was revealed by the typical bands on the adsorbent's spectra at 3419 and 3470 cm^{-1}. At 1690 cm^{-1}, there were no C=O bands in the spectrum of GP/MIL-53(Cr), and the $-NH_2$ bands of MIL-53(Cr) reduced dramatically, thus signifying a major dehydration/condensation process between the $-NH_2$ and −CHO groups. In GP/MIL-53(Cr), a strong and broadband near 3418 cm^{-1} suggest the presence of $-NH_2$ and −NH− groups. Furthermore, the peaks at 1690 cm^{-1} are due to −C=O and C=C (aromatic ring) and −C=O stretching bonds, respectively. The CO and C=O peaks faded when GO was treated with MIL-53(Cr), and the new peaks developed were ascribed to the stretching vibrations of NH (amine group) and CH. Additionally, the triazine ring's C=N stretching vibrations at 1557, 1482, and 1351 cm^{-1} revealed that the GP triazine units had been completely absorbed into the adsorbent-structure [2,21,22]. The broad peak at 1556 cm^{-1} is attributed to hydroxyl (OH) stretching in the case of GP. It was confirmed that the desired GP/MIL-53(Cr) was effectively synthesized.

The Raman spectra of the adsorbents are as shown in Fig. 4b. The two peaks at 1346 cm^{-1} and 1577 cm^{-1} correspond to the D/G bands. The band D shows the defects of C atomic lattice, while the G band displays the sp2 hybridized carbon in-plane stretching vibration. The relative content or disorder degree of defects in the carbonaceous materials was investigated using the intensity ratio of these two bands (ID/IG) [17,20]. In Fig. 4b, the ratio of ID/IG values of A (600.0), B (650.0), and C (700.0) are 3.610, 3.620, and 3.730, respectively, thus revealing that an increase in the carbonization temperature can result into an increase in the formation of defective sites [31]. The site defects had a lot of delocalized electrons; hence, there were a lot of active sites. The defect density increased with increased temperature which resulting in the re-fabrication of the carbon skeleton at high temperatures due to N_2 atomic doping, which improved the defect density [5,22].

3.1.4. XRD patterns

Figure 5 shows the crystalline features obtained from XRD analysis which helped to identify the crystalline structures of the synthesized hybrid adsorbent as well as their parent materials. The main peaks of GP/MIL-53, MIL-53(Cr), and GP at 2θ are 35.8°, 9.98°,

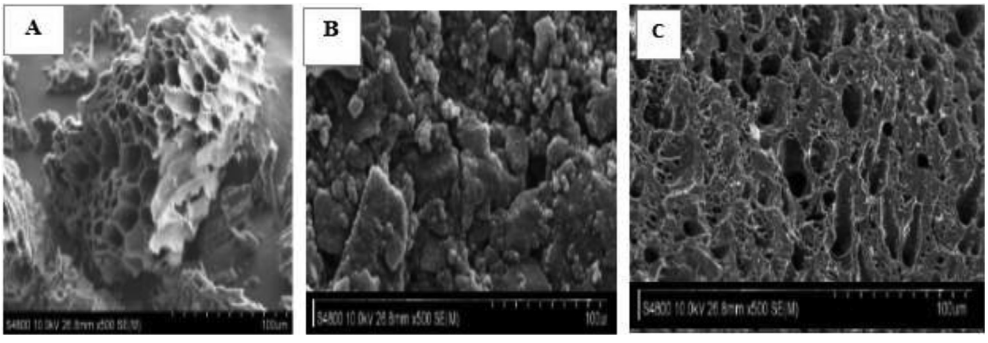

Fig. 2. SEM images of (a) cationic graphene oxide-based polymer composite (modified), (b) MIL-53(Cr), and **(c) GP**/MIL-53(Cr).

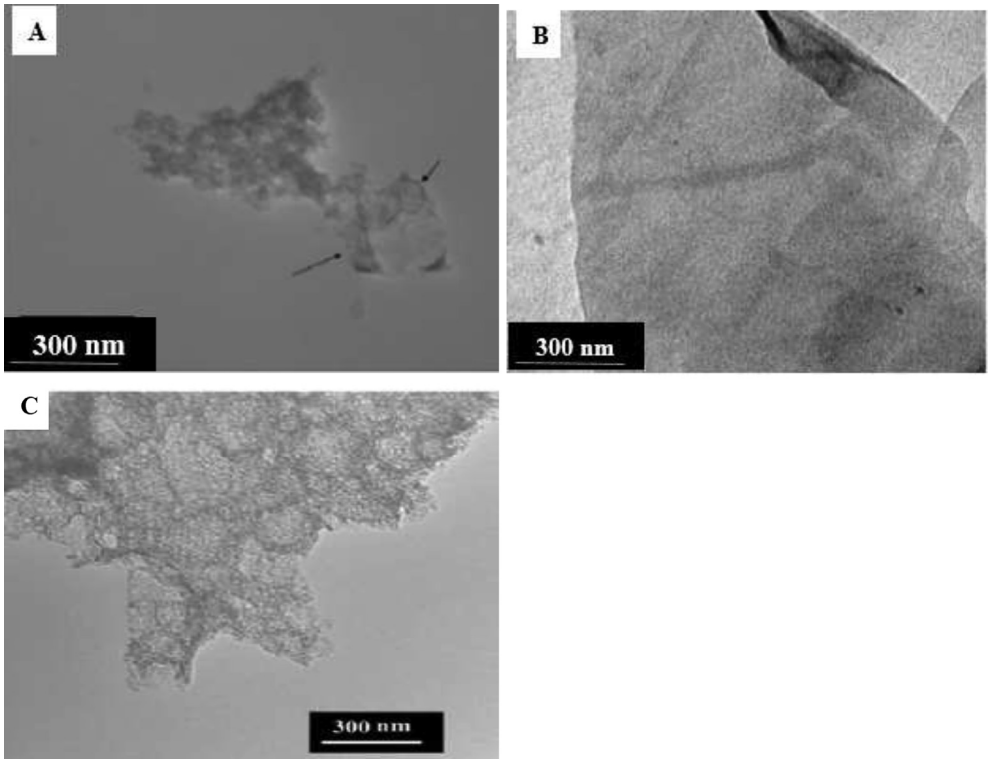

Fig. 3. TEM Images of (a) cationic Graphene based polymer composite modified (b) MIL-53(Cr) **(c) GP**/MIL-53(Cr).

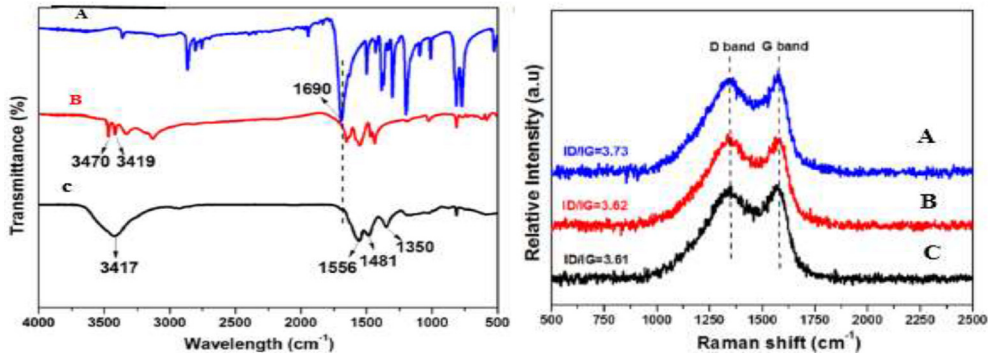

Fig. 4. (a) FT-IR; (b) Raman spectra of the adsorbents: **A- GP**/MIL-53(Cr); **B**- MIL-53(Cr); **C- GP**.

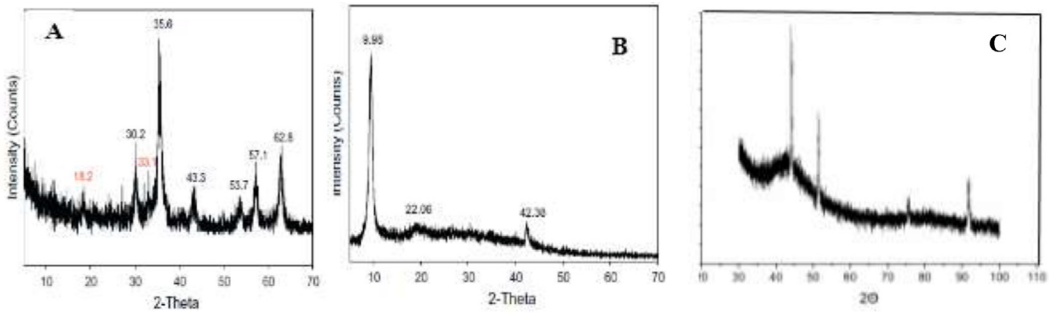

Fig. 5. XRD pattern of A - GP/MIL-53(Cr); B - MIL-53(Cr); C - GP.

7.37°, respectively. This result indicates that doping MIL-53(Cr) with graphene composites did not disrupt the crystal structure in anyway. Also, it can be seen that GP composite has the same distinctive peaks of MIL-53(Cr); however, the peak' intensities increased after modification of the adsorbents, thus indicating that the GP composite/MIL-53 was been successfully synthesized. These outcomes corroborate the works of Refs [14,20,23,30] which comprise of an effective decoration of MOFs. No impurity was observed in the peaks, which is an indication that the product is pure.

3.1.5. The XPS adsorbents spectrum

The XPS study explains the mechanism of 2,4-DCP adsorption on the cationic graphene-based polymer composite/MIL-53(Cr). The chemical state of GO species in MIL-53(Cr) before and after reaction was examined. Figure 6a–e demonstrates the XPS spectrum of GP/MIL-53(Cr) before and after 2,4-DCP adsorption. The peaks were clearly identified at 385 and 395 eV binding energy for MIL-53(Cr)$_{7/2}$ and MIL-53(Cr)$_{5/2}$, respectively. This was similar to the results presented by Refs [9,12]. The obtained peaks showed the presence of MOF-MIL-53(Cr). The prominent peaks in the C 1s spectra of the adsorbents before and after 2,4-DCP adsorption were deconvoluted as follows: in Fig. 5c, the C–C carbides (283.0 eV), non-oxygenated C–C bond (285.0), C–O bond (286.0), and O=C bond are all non-oxygenated C–C bonds [1,10,22]. After 2,4-DCP adsorption, all oxygenation bonds (i.e., O=C C–O, and C–O–C bonds) of GP/MIL-53(Cr) changed to higher energy levels than the non-oxygenated C–C bonds, as shown in Fig. 5c. MIL-53(Cr), on the other hand, did not show any major changes in its present form. As a result, the oxygenation bonds of the GP/MIL-53(Cr) were chemically linked to 2,4-DCP, thus showing some measure of agreement with the results obtained from the FTIR. The outcome of FTIR/XPS confirms that the GP/MIL-53(Cr) can effectively capture 2,4-DCP as a result of the interactions between 2,4-DCP and the adsorbent-oxygenated groups.

3.1.6. Adsorbents pore size distribution

N_2 sorption was used to analyze the pore structure of [GP/MIL-53(Cr)], and the related pore size distributions were integrated. The IUPAC (**International Union of Pure and Applied Chemistry**) system of classification was used to classify the GP/MIL-53(Cr) curve as type-IV, as shown in Fig. 7. At relatively low pressures, the isotherm has a high upward-sloping trend, thus indicating the existence of microporous networks [12]. This finding is supported by the GP/MIL-53(Cr) pore size distribution plot. The GP/MIL-53(Cr) exhibits apparent capillary condensation at medium relative pressure, thus indicating the presence of mesoporous networks [13]. The steady increase in N_2 adsorption at higher pressures implies

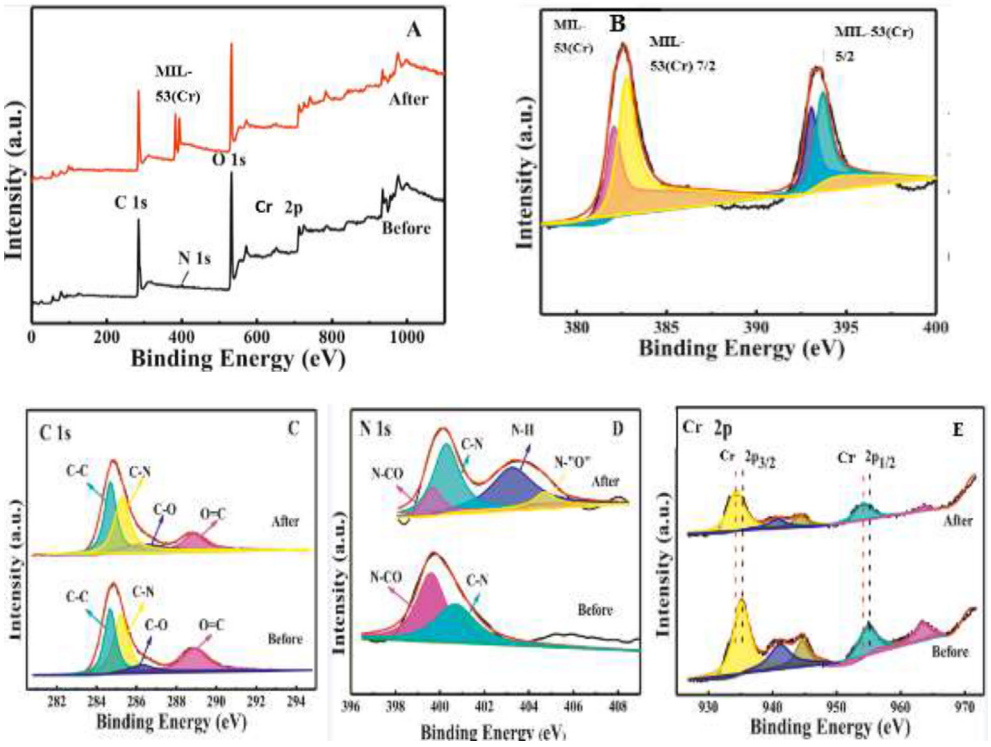

Fig. 6. XPS survey spectrum of the adsorbents before and after 2,4-dichlorophenol adsorption.

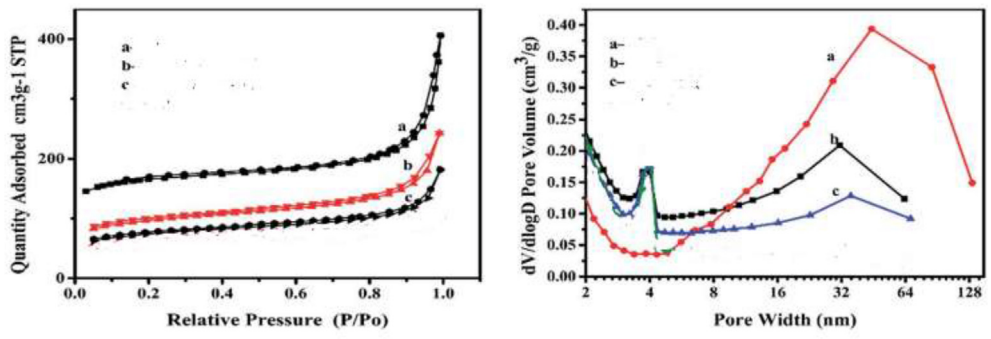

Fig. 7. Pore size distribution of the adsorbents.

Table 2
Porous structural parameters for GP, MIL-53(Cr), and GP/MIL-53(Cr).

Adsorbent(s)	S_{BET} (m^2g^{-1})	S_{micro} (m^2 g^{-1})	V_P (cm^3 g^{-1})	V_{micro} (cm^3 g^{-1})	V_{meso} (cm g^{-1})
GP	404	182	1.10	0.05	0.91
MIL-53(Cr)	583	322	1.12	0.10	0.92
GP/MIL-53(Cr)	815	493	1.17	0.20	1.21

the existence of slit-like holes originating from the layered structure. Furthermore, the pore size distribution curve (Fig. 7b) shows that the GP/MIL-53(Cr) has a restricted pore size distribution, with the largest peak centered at roughly 51.7 nm using the BJH desorption technique. Table 2 shows the pore volume and BET surface areas of the GP/MIL-53(Cr) and other adsorbents.

3.2. Adsorption studies

3.2.1. Adsorbents dosage

To identify the optimum dosage of the GP, MIL-53(Cr), and GP/MIL-53(Cr), the effects of adsorbent dosage on the adsorption capacity and removal ratio were studied, as presented in Fig. 8. (a, b, and c). The adsorbents' dosage increased from 10.0 mg/L to 400 mg/L, and the adsorption of 2,4-DCP on the GP, MIL-53(Cr), and GP/MIL-53(Cr) increased from 210 to 396 mg/g, 199–370 mg/g, and 99–499 mg/g, respectively. These adsorbents displayed improved adsorption capacity for 2,4-DCP; however, GP/MIL-53(Cr) showed an excellent adsorption capacity. Furthermore, the adsorption capacities described for other adsorbents reported are Cr-MOF (381.1 mg/g) [25], Zr-MOF (251.6 mg/g [14] and AC (327.5 mg/g [33]. However, the GP/MIL-53(Cr) displayed a larger surface area (815 m^2 g^{-1}) when compared to those of GP and MIL-53(Cr) as presented in Table 2, which may perhaps be responsible for its higher adsorption capacity. According to the data from zeta potential, lower adsorption capacity results are attributable to electrical repulsion. Furthermore, rather than the physical surface area, electrical attraction is the primary mechanism of 2,4-DCP adsorption. FTIR/XPS measurements were used to determine the unique adsorption mechanism. Interestingly, an increase in the adsorbent dose increases the removal ratio of 2,4-DCP, and the maximum percent removals of 2,4-DCP were observed to be 71.0%, 63.1%, and 95.7% for GP, MIL-53(Cr), and GP/MIL-53(Cr), respectively. For all the three adsorbents, the recorded adsorptive capacities are measures of their initial total number of vacant sites available for adsorption, which comprises the number of active sites occupied by 2,4-DCP and the number of vacant sites which were unoccupied by the adsorbate after contact. This then informs that the volume of the occupied pores per adsorbent can be related to the concentration of 2,4-DCP at their pore sites which is responsible for the difference in the adsorptive capacities and removal efficiencies of 2,4-DCP by the adsorbents [6].

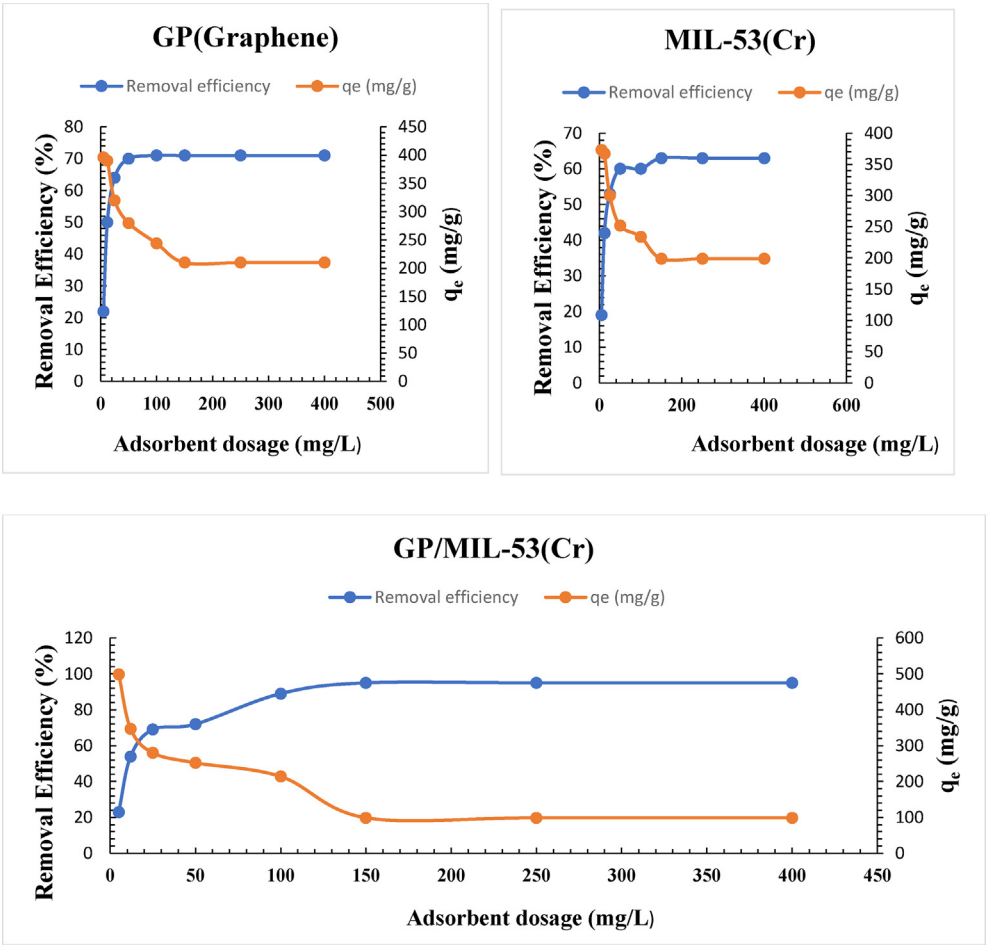

Fig. 8. Dosage of adsorbents for 2,4-DCP removal.

3.2.2. Effect of initial pH

pH is a significant determinant in adsorptive performance of adsorbents since its impact on the surface charge of the adsorbents and the ionic species of 2,4-DCP, and some adsorbents have an attraction for H^+ or OH^- ions, which can cause variations in adsorption capacity and solubility by directly affecting the pH of the solution [7,15,19]. The adsorption process is further influenced by the H^+ and OH^- ions, which dissociate the functional groups on the adsorbent and adsorbate. The adsorption of phenol and its derivatives on GP/MIL-53(Cr) is facilitated by a "donor–acceptor complex" mechanism in which the carbonyl surface/O_2 groups act as electron donors and the aromatic rings of the solute act as acceptors [14,22]. Many oxygenated functional groups, for example, hydroxyl, carbonyl, formyl, carboxyl, and phenyl may exhibit positive or negative characteristics during adsorption on the adsorbent GP/MIL-53(Cr) surface. The pH of adsorbate solutions can influence their chemical properties, which, however, impact on the adsorption process. As a result, in the adsorption of 2, 4-DCP, the pH of the adsorption medium is an important parameter.

Figure 9b shows a wide pH range between 1.0 and 10.0. The maximum removal efficiencies of the adsorbate by each adsorbent GP, MIL-53(Cr), and GP/MIL-53(Cr) were obtained at pH of 10 giving values of 66%, 84%, and 95%, respectively. Thus, the ability of the adsorbent to remove 2,4-DCP mainly comes from the presence of GP/MIL-53(Cr), and a small quantity of GP helps to improve the removal efficiency of the adsorbate. Another reason for the high removal efficiency recorded for GP/MIL-53(Cr) may be attributed to the property and structure of GP/MIL-53(Cr), and pH which may have altered the amount of active ingredients in GP/MIL-53(Cr). The ionic states of the carboxyl and hydroxyl groups on GP/MIL-53(Cr) surface are additional factors that affect the adsorption process.

In summary, the removal efficiency and zeta potential of GP and MOF tend to increase as the pH increases [Fig. 9a]. The adsorbents' performance (i.e., removal ratio and adsorption capacity) was poorer at a low pH than it was at a pH of 6–10. This might be the result of electrostatic forces causing complexation. Because of the competition of 2,4-DCP, a majority of H^+ at a low pH occupies the active sites of the GP/MIL-53(Cr), leading to decreased removal ratios and adsorption capacities. Furthermore, as the pH increased, the hydroxyl and carboxyl groups on the surface of GP/MOF were continually deprotonated, leading to a progressively negative surface charge [24,28,34]. Since there is a robust complexation by protonated hydroxyl and carboxyl groups, the negatively charged surface charge of GP/MIL-53(Cr) efficiently adsorbed the positively charged 2,4-DCP, thus resulting in improved adsorption capacity and removal ratio. Hence, the adsorption of 2,4-DCP by GP/MIL-53(Cr) mainly occured by electrostatic interactions.

3.2.3. Influence of contact time

Generally, a longer contact time influences higher adsorption of 2,4-DCP. Absorption consumes a lot of time; thus, an increase in contact time was advantageous for the appropriate loading of 2,4-DCP on the adsorption sites of GP, MIL-53(Cr), and GP/MIL-53(Cr). GP/MIL-53(Cr) gave a longer contact time than other adsorbents analyzed with maximum removal efficiency of 2,4-DCP at 98.4%, compared to GP and MIL-53(Cr) with removal efficiency of 55% and 63%, respectively, at shorter contact time (Fig. 10). The adsorption rate increases fast with time in the first zone, due to the existence of many active adsorption surface sites [5,18]. The initial adsorption sites for 2,4-DCP in GP/MIL-53(Cr) were satisfactory. With the passage of time, additional pore sites were occupied, and the system eventually attained its saturation point in terms of adsorption capacity. The adsorption rate gradually slows down as time passes. This suggests that active sites on the surface of the adsorbent are being occupied at a higher rate. Finally, as time passes, the adsorption rate approaches a constant, and equilibrium is attained. Similarly, the optimum pecentage removal efficiency for GP, MIL-53(Cr), and GP/MIL-53(Cr) in 2,4-DCP removal are 62, 69, and 94 %, respectively. Beyond 120 min, no significant increase was observed in the removal efficiency, thus implying the saturation of GP/MIL-53(Cr) adsorptive sites with 2,4-DCP.

In Fig. 10, the GP is made up of one layer/component so the diffusion of 2,4-DCP molecules through the pores is monolayer owing to the near distance of separation between the end of one pore at the base of the material to another at the surface. Hence, the diffusion of 2,4-DCP was fastest in GP compared to MIL-53(Cr) and GP/MIL-53(Cr) within the first 40 min. However, after 40 min, the adsorbent got saturated with 87% which led to no further removal of 2,4-DCP at 80 min.

For the MIL-53(Cr), which also performed better than the GP/MIL-53(Cr), within the first 40 min, the number of layers are two comprising of MIL and 53(Cr); hence, the distance of separation for 2,4-DCP diffusion through the layers from the base to the top layer had a mixture of MIL and 53(Cr) which resulted in the slow diffusion of molecules through the layers within the first 40 min, and thereafter it was able to adsorb more 2,4-DCP (i.e., 89 % compared to 87% for GP at 80 min which is the saturation time).

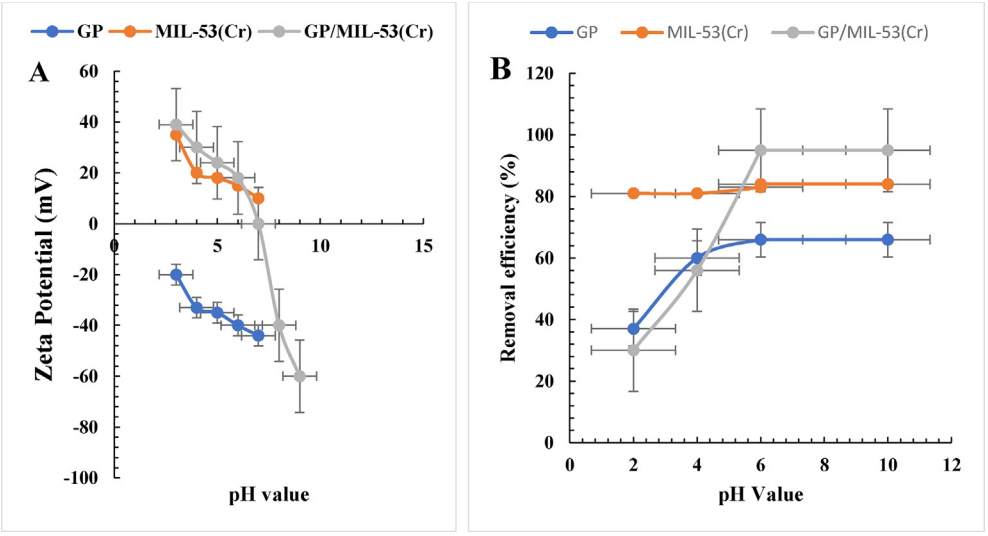

Fig. 9. (a) Zeta potential values at several Ph; (b) removal efficiency at several pH values.

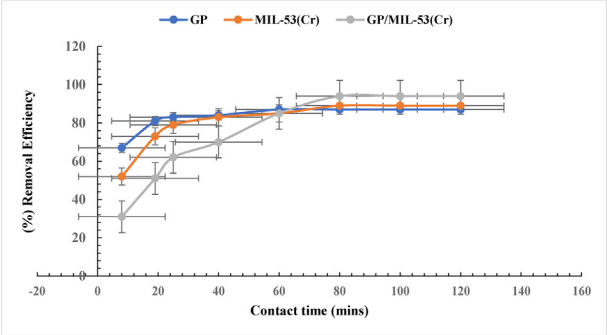

Fig. 10. Effect of contact time on the removal efficiency.

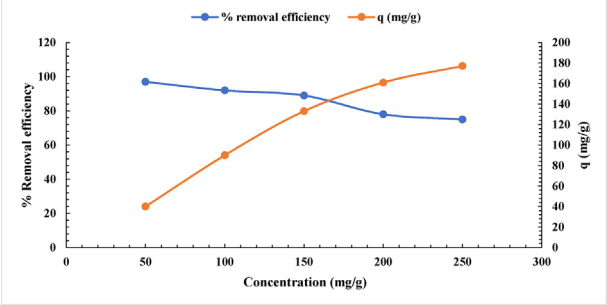

Fig. 11. Effect of initial 2,4-dichlorophenol concentration.

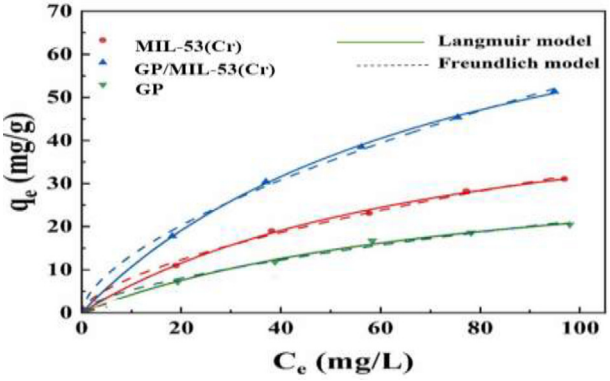

Fig. 12. Langmuir and Freundlich isotherm of different adsorbents.

However, considering the GP/MIL-53(Cr), there are three components (three layers) making up this material; hence, the cumulative distance traveled by 2,4-DCP through this mixed matrix system, caused the initial slow diffusion of 2,4-DCP within the first 40 min. Thereafter, owing to the availability of more pores relative to the GP and MIL-53(Cr) adsorbents, there was net diffusion of molecules which led to the increased concentration/adsorption of 2,4-DCP; hence, within a saturation time of 80 min, the net absorption of 2,4-DCP was 94%.

3.2.4. Effect of initial 2,4-dichlorophenol concentration

Figure 11 shows the effect of initial concentration of 2,4-DCP (50−250 mg/L) on percentage removal and adsorption capacity, as well as their relationship with time, keeping the other parameters constant. The initial concentration of 2,4-DCP increases from 50.0 to 250.0 mg/L, with increase in the adsorption capacity from 41.2 to 177.3 mg/g at an equilibrium time of 100 min. Since there are more 2,4-DCP molecules that can be adsorbed on the GP/MIL-53(Cr) composite at higher concentrations, this trend is expected [17,18]. As the initial concentration of 2,4-DCP increased from 50 to 250 mg/L, the percentage removal decreased from 97.0 to 75.01%. This may be attributed to the presence of high adsorbent molecules in the active site ready to accept more 2,4-DCP molecules especially at low concentration, thus resulting in the high saturation of the site which makes it lose its ability to adsorb more 2,4-DCP molecules at higher concentrations.

3.3. Adsorption isotherms

3.3.1. Adsorption isotherms and thermodynamics

The adsorption performance of 2,4-DCP onto GP, MIL-53(Cr), and GP/MIL-53(Cr) was considered using the isotherms of Freundlich and Langmuir. The Langmuir isotherm assumes homogenous adsorption on a monolayer surface with a finite number of adsorptive sites. The isotherms equation is shown in Table 1. The linear plots of both isotherms are shown in Fig. 12. The (R^2) for Langmuir and Freundlich isotherms are 0.999 and 0.998, signifying that both models can adequately describe the adsorption of 2,4-DCP onto GP, MIL-53(Cr), and GP/MIL-53(Cr).

Furthermore, the Freundlich's n value of 1.69 demonstrates high affinity between the 2,4-DCP and GP/MIL-53 (Cr). The maximal adsorption capacities of 2,4-DCP onto GP, MIL-53(Cr), and GP/MIL-53(Cr) are 47.9 mg/g, 55.7 mg/g, and 98.2 mg/g, respectively, according to the Langmuir isotherm (Table 3). Furthermore, the highest adsorption capacity of 2,4-DCP onto GP, MIL-53(Cr), and GP/MIL-53(Cr) were compared to that of previously published adsorbents [5,21,30,32]. The comparison (Table 4) clearly shows that

Table 3
Langmuir and Freundlich isotherm of different adsorbents.

	Langmuir isotherm			Temp. (28 °C)	Freundlich isotherm		
Adsorbent used	q_m (mg/g)	$K_L\left(\frac{L}{mg}\right)$	R^2	28.0 °C	N	$K_F\left(\frac{mg}{g}\right)$	R^2
GP	47.9	0.0140	0.995	28.0 °C	1.61	0.39	0.990
MIL-53(Cr)	55.7	0.0127	0.991	28.0 °C	1.49	1.84	0.982
GP/MIL-53(Cr)	98.2	0.0148	0.999	28.0 °C	1.69	2.08	0.998

Table 4
Review of some previous works on Freundlich and Langmuir isotherms constants for the removal of 2,4-DCP.

Adsorbent	q_m (mg/g)	b (L/mg)	k_F (L/g)	n	Ref.
Oil palm empty fruit branches	27.25	0.56	3.42	2.0	[5]
Activated bamboo charcoal	45.25	2.6	20.48	2.27	[3]
Palm pith carbon	19.2	0.73	2.45	1.21	[1]
Immobilized Phanerochaete chrysosporium	7.15	0.039	0.52	1.75	[9]

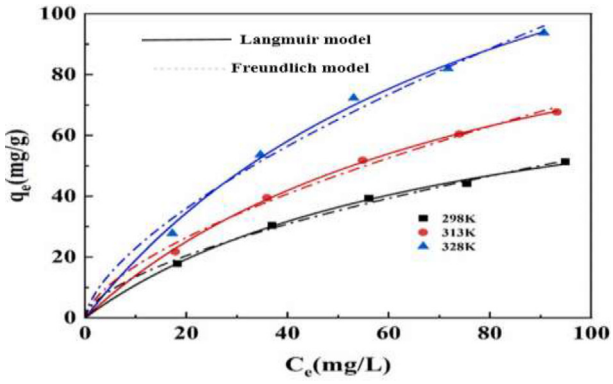

Fig. 13. Langmuir and Freundlich isotherm at different temperatures for 2,4-DCP onto GP/MIL-53(Cr).

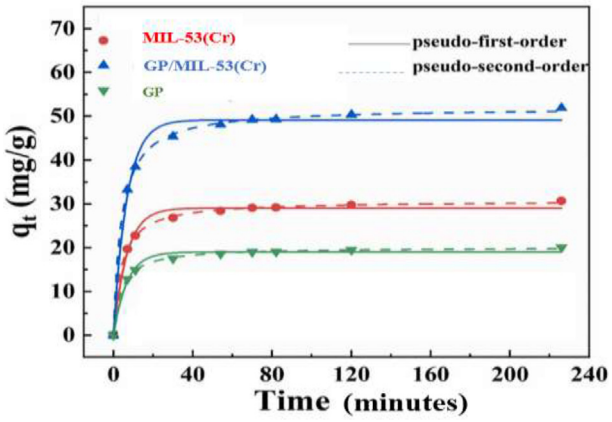

Fig. 14. Kinetic model on GP, MIL-53(Cr) and GP/ MIL-53(Cr) Adsorption.

Table 5
Thermodynamic adsorption of 2,4-DCP onto GP/MIL-53(Cr).

Adsorbent(s)	Temp. (K)	$\Delta G\left(\frac{kJ}{mol}\right)$	$\Delta H\left(\frac{kJ}{mol}\right)$	$\Delta S\left(\frac{J}{K.mol}\right)$
GP/MIL-53(Cr)	298	−13.95	18.37	114.2
	313	−14.99		
	328	−19.02		

GP/MIL-53(Cr) has a higher adsorption capacity than other previously stated adsorbents. This is likely due to the fact that GP/MIL-53(Cr) can interact with 2,4-DCP in a variety of ways: (I) electrostatic interaction/attraction between 2,4-DCP and GP/MIL-53(Cr); (ii) conjugation among GP/MIL-53(Cr) benzene rings and aromatic 2,4-DCP; and (iii) hydrogen bonding between GP/MIL-53(Cr) and 2,4-DCP. As a result, the Langmuir model fits the data better than the Freundlich model, showing that the adsorption is monolayer.

Gibbs free energy (ΔG) enthalpy (ΔH) and entropy (ΔS) are the adsorption thermodynamic parameters presented in Table 1. Negative ΔG values suggested spontaneous adsorption. When ΔH becomes positive, it specifies that the adsorption is endothermic. In addition, when ΔS is positive, it shows an increase in disorderliness at the solid/solution interface [14]. Adsorption thermodynamics at different temperatures for 2,4,-DCP onto GP/MIL-53(Cr) are illustrated in Fig. 13 and Tables 5 and 6.

3.3.2. Adsorption kinetics

The pseudo-first and pseudo-second-order were used to evaluate the kinetic mechanism and adsorption rate of GP/MIL-53(Cr). Figure 14 depicts the fitting curves, while Table 1 includes the kinetic parameters. The three (GP, MIL-53(Cr), and GP/MIL-53(Cr) modified adsorbents' adsorption capabilities increased sharply during the first 20 min and attained adsorption equilibrium at around 40 min. Owing to its $R^2 > 0.999$, the pseudo-second order for GP/MIL-53(Cr) fits the experimental data more accurately. Hence, the pseudo-second-order kinetic model is suitable in describing the adsorption of 2,4-DCP onto GP/MIL-53(Cr), indicating that chemical adsorption is the rate-limiting step. Furthermore, the computed qe values for GP, MIL-53(Cr), and GP/MIL-53(Cr) were 16.3 mg/g, 34.5 mg/g, and 59.06 mg/g, respectively. The outcome further shows that 2,4-DCP adsorption on GP/MIL-53(Cr) follows a pseudo-second-order kinetic model. Additionally, MIL-53(Cr) has a lesser K_2 value (3.13×10^{-4}) than GP/MIL-53(Cr), thus suggesting that GP/MIL-53(Cr) has a higher affinity for 2,4-DCP than MIL-53 (Cr), which resulted in an increase in the adsorption rate of 2,4-DCP. According to the results, the addition of GP to MIL-53(Cr) provides additional adsorption sites for GP/MIL-53(Cr).

3.4. Proposed mechanism for adsorption of 2,4-dichlorophenol

To further explain the adsorption mechanism of **2,4-DCP** onto GP/MIL-53(Cr), FTIR and XPS were used to study the functional groups on the GP/MIL-53(Cr) surface for **2,4-DCP** adsorption. Although this has been explained in the previous section. However, the presence of PMMA in GP/MIL-53(Cr) may have also facilitated the electrostatic attraction between GP/MIL-53(Cr) and **2,4-DCP.** Considering the PMMA in GP/MIL-53(Cr), it is proposed that there will be the formation of H_2 bond between GP/MIL-53(Cr) composite and 2,4-DCP, leading to high adsorption of 2,4-DCP. Furthermore, the π-π staking interaction between aromatic rings **2,4-DCP** and the benzene carboxylic groups of MOFs showed high adsorption capacity of GP/MIL-53(Cr) (Fig. 15). Another possible mechanism is the availability of high surface area and pore structure, where the **2,4-DCP diffused and interacted with the** GP/MIL-53(Cr) asre shown in Fig. 15; thus, the **2,4-DCP ions** combine with the active sites of −COOH and −OH in GP/MIL-53(Cr). More works are needed in detail to characterize the adsorption mechanism.

Table 6
Parameter for adsorption kinetics of pseudo-first and second order on GP/MIL-53(Cr).

Adsorbent(s)	Kinetics of pseudo-first order				Kinetics of pseudo-second order		
	$q_{e,exp}\left(\frac{mg}{g}\right)$	$q_{1e,cal}\left(\frac{mg}{g}\right)$	$k_1(min^{-1})$	R^2	$q_{2e,cal}\left(\frac{mg}{g}\right)$	$k_2\left(\frac{g}{mg.min}\right)$	R^2
GP	14.5	14.0	0.032	0.961	16.3	2.83×10^{-4}	0.995
MIL-53(Cr).	33.2	32.8	0.049	0.970	34.5	3.13×10^{-4}	0.998
GP/MIL-53(Cr).	56.84	55.5	0.075	0.975	59.06	2.21×10^{-4}	0.999

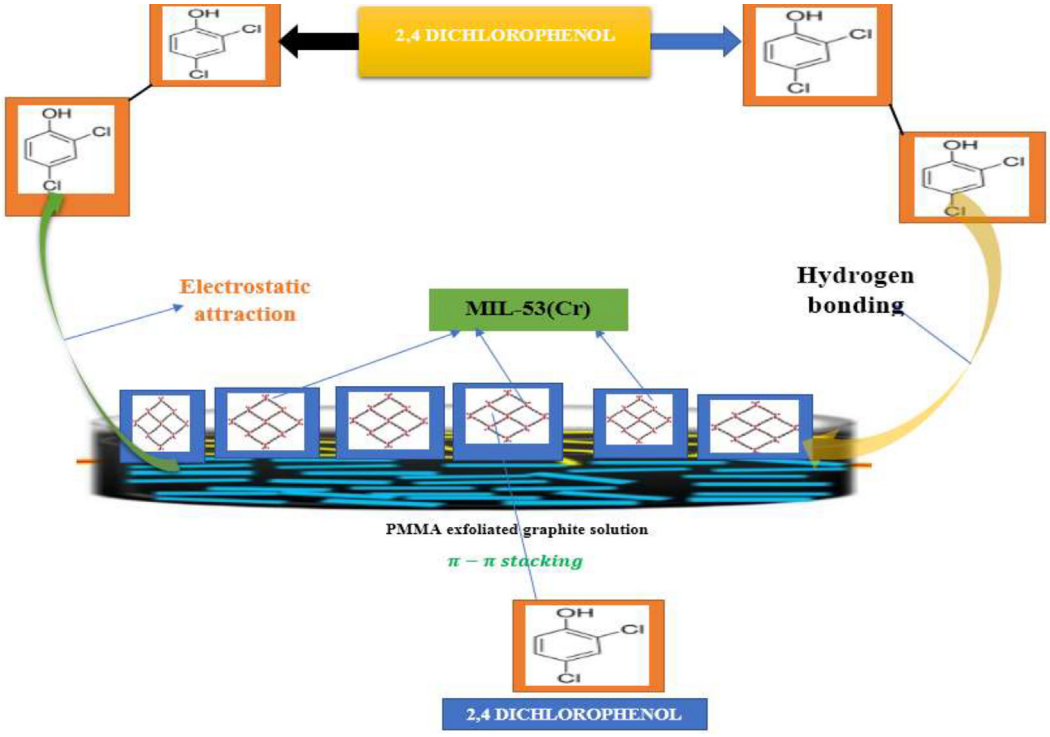

Fig. 15. Schematics of the proposed mechanism for adsorption of 2,4-DCP.

3.5. Mineralization of 2,4-DCP

The degree of mineralization is a key measure of the reaction system's feasibility in wastewater treatment. Generally, the pollutants' mineralization efficiency is lower than their degradation efficiency [5,25]. The authors considered the mineralization of 2,4-DCP at different intervals as shown in Fig. 16 to fully understand the total degradation of 2,4-DCP in the reaction system. As a result, experiments were conducted at lower 2,4-DCP doses. The study demonstrates that at an initial concentration of 1×10^{-5} M, 2,4-DCP was fully eliminated in 200 min, and the solution was totally mineralized in 4 h. This finding supports the hypothesis that the adsorption and mineralization rate of GP/MIL-53(Cr) are inversely proportional to the 2,4-DCP initial concentration.

Mineralization of 2,4-DCP entails mineralization of all intermediates produced during its oxidation. Investigations with 2,4-DCP revealed an almost total mineralization (95%), thus suggesting that GP/MIL-53(Cr) is a suitable adsorbent for achieving complete mineralization.

3.6. Adsorbent rreusability

From an economic standpoint, the adsorbent's recyclability is critical. The spent GP/MIL-53(Cr) was recovered after adsorption by centrifugation at 5000 rpm for 20 min. The adsorbed 2,4 DCP was then desorbed with 1 M CH_3OH/NaCl and the adsorbent was dried at 70 °C for recycling. After adsorption/desorption cycles, 99.6% removal efficiency was obtained which is relatively high (Fig. 17), thus demonstrating the great feasibility of GP/MIL-53(Cr) in real

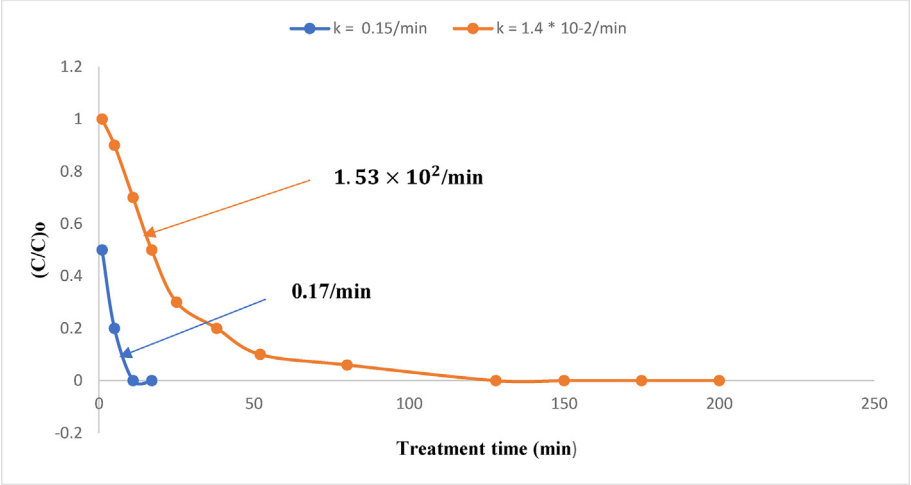

Fig. 16. Complete mineralization of 2,4-DCP.

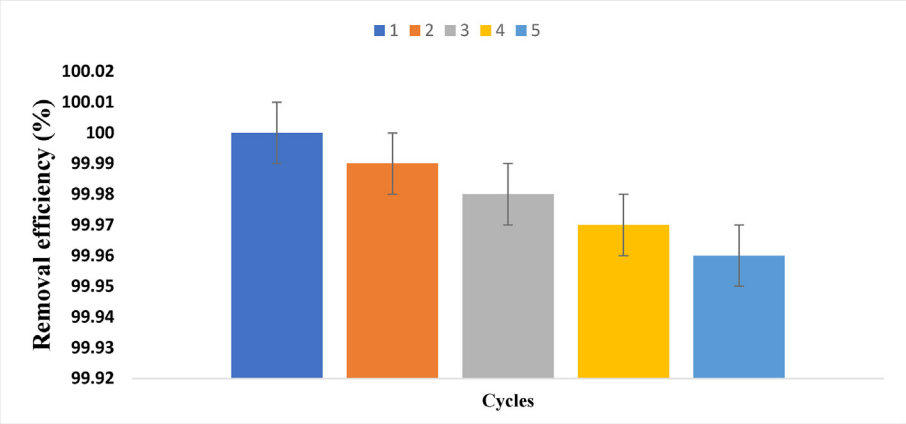

Fig. 17. Removal efficiency of each cycle.

situations. The adsorbent that was regenerated was activated for 12 h in a vacuum at 150 °C.

4. Conclusion

A simple one-pot solvothermal synthesis process was used to successfully synthesize GP/MIL-53(Cr), a novel ternary composite material. MIL-53(Cr) adsorption was primarily anchored on PMMA-GO surface, and the composite showed a stable structure before and after adsorption. The adsorbent was easily removed from the solution, and the adsorption capacity was increased by using GO/PMMA. Initial pH, solution concentration, and contact time all influenced the adsorption capacity of the adsorbent. The adsorption data adequately suit the Langmuir isotherm and pseudo-second-order model according to the experimental results. The estimated thermodynamic characteristics showed that the adsorption was spontaneous, endothermic, and efficient. Therefore, GP/MIL-53(Cr), a novel adsorbent can efficiently remove 2,4-DCP from aqueous solution.

Credit author statement

Babalola Aisosa Oni: Conceived the idea, carried out the experimentation, and made the first draft copy of the manuscript. **Samuel Eshorame Sanni:** Made useful contributions at different stages of the research and involved in recomposing key sections of the manuscript.

Declaration of competing interest

The authors declare that they have no known competing financial interests or personal relationships that could have appeared to influence the work reported in this paper.

References

[1] O.G. Abatan, B.A. Oni, O. Agboola, V. Efevbokhan, O.O. Okiki Abiodun, Production of activated carbon from African star apple seed husks, oil seed and whole seed for wastewater treatment, J. Clean. Prod. 232 (2019) 441–450.
[2] O.G. Abatan, P.A. Alaba, B.A. Oni, K. Akpojevwe, V. Efeovbokhan, F. Abnisa, Performance of eggshells powder as an adsorbent for adsorption of hexavalent chromium and cadmium from wastewater, SN Appl. Sci. 2 (2020) 1996, https://doi.org/10.1007/s42452-020-03866-w.
[3] I. Ali, T.A. Khan, M. Asim, Removal of arsenic from water by electrocoagulation and electrodialysis techniques, Separ. Purif. Rev. 240 (2011) 25–42.
[4] A. Bianco, H.-M. Cheng, T. Enoki, Y. Gogotsi, R.H. Hurt, N. Koratkar, et al., All in the graphene family – a recommended nomenclature for two-dimensional carbon materials, Carbon 65 (2013) 1–6.
[5] Y. Cui, Z. Zeng, J. Zheng, Z. Huang, J. Yang, Efficient photodegradation of phenol assisted by persulfate under visible light irradiation via a nitrogen-doped titanium-carbon composite, Front. Chem. Sci. Eng. (2021) 1–9, https://doi.org/10.1007/S11705-020-2012-Z.
[6] Y. Cui, B. Li, H. He, W. Zhou, B. Chen, G. Qian, Metal–organic frameworks as platforms for functional materials, Acc. Chem. Res. 49 (2016) 483–493.
[7] H.H. Dang, D.T.C. Nguyen, T.T. Nguyen, T.T.T. Nguyen, D.-V.N. Vo, T.D. Nguyen, T. Lee, T.V. Tran, Zeolitic-imidazolate framework-derived N-self-doped porous carbons with ultrahigh theoretical adsorption capacities for tetracycline and ciprofloxacin, J. Environ. Chem. Eng. 9 (1) (2021) 104938, https://doi.org/10.1016/j.jece.2020.104938.
[8] X. Gong, G. Liu, Y. Li, D.Y.W. Yu, W.Y. Teoh, Functionalized-graphene composites: fabrication and applications in sustainable energy and environment, Chem. Mater. 28 (22) (2016) 8082–8118.
[9] B. Han, E. Zhang, G. Cheng, L. Zhang, D. Wang, X. Wang, Hydrothermal carbon superstructures enriched with carboxyl groups for highly efficient uranium removal, Chem. Eng. J. 338 (2018) 734–744.
[10] Y. Hu, D. Chen, S. Wang, R. Zhang, Y. Wang, M. Liu, Activation of peroxymonosulfate by nitrogen-doped porous carbon for efficient degradation of organic pollutants in water: performance and mechanism, Separ. Purif. Technol. 280 (2022) 119791, https://doi.org/10.1016/j.seppur.2021.119791.
[11] C. He, W. Xia, C. Zhou, D. Huang, C. Zhang, B. Song, Y. Yang, J. Li, X. Xu, Y. Shang, L. Du, Rational design to manganese and oxygen co-doped polymeric carbon nitride for efficient nonradical activation of peroxymonosulfate and the mechanism insight, Chem. Eng. J. 430 (2022) 132751.
[12] N. Jaafarzadeh, F. Ghanbari, M. Ahmadi, Efficient degradation of 2,4-dichlorophenoxyacetic acid by peroxymonosulfate/magnetic copper ferrite nanoparticles/ozone: a novel combination of advanced oxidation processes, Chem. Eng. J. 320 (2017) 436–447.
[13] D.J. Kim, J.W. Yoon, C.S. Lee, Y.-S. Bae, J.H. Kim, C,ovalent organic framework-derived microporous carbon nanoparticles coated with conducting polypyrrole as an electrochemical capacitor, Appl. Surf. Sci. 439 (2018) 833–838, https://doi.org/10.1016/j. apsusc.2018.01.103.
[14] S. Li, Y. Chen, X. Pei, S. Zhang, X. Feng, J. Zhou, B. Wang, Water purification: 644 adsorption over metal-organic frameworks, Chin. J. Chem. 34 (2) (2016) 175–185.
[15] C. Liu, L.-Q. Yu, Y.-T. Zhao, Y.-K. Lv, Recent advances in metal-organic frameworks for adsorption of common aromatic pollutants, Microchim. Acta 185 (7) (2018) 342, https://doi.org/10.1007/s00604-018-2879-2.
[16] S. Luo, J. Wang, MOF/graphene oxide composite as an efficient adsorbent for the removal of organic dyes from aqueous solution, Environ. Sci. Pollut. Res. (2017), https://doi.org/10.1007/s11356-017-0932-z.
[17] Z.M. Lv, H.Y. Wang, C.L. Chen, S.M. Yang, L. Chen, A. Alsaedi, et al., Enhanced removal of uranium(VI) from aqueous solution by a novel Mg-MOF-74-derived porous MgO/carbon adsorbent, J. Colloid Interface Sci. 537 (A1–A10) (2019a).
[18] A.G. Márquez, A. Demessence, A.E. Platero-Prats, D. Heurtaux, P. Horcajiada, C. Serre, J.S. Chang, G. Férey, V.A. de la Peña-O'Shea, C. Boissière, D. Grosso, C. Sanchez, Green microwave synthesis of MIL- 100(Al, Cr, Fe) nanoparticles for thin-film elaboration, Eur. J. Inorg. Chem. 201 (2012) 5165–5174.
[19] B.A. Oni, S.E. Sanni, S.O. Dahunsi, B.C. Egere, Decaffeination of wastewater using activated carbon produced from velvet tamarind-pericarp (*Dialium Guineense*), Int. J. Phytoremediation (2021), https://doi.org/10.1080/15226514.2021.1950118.
[20] B.A. Oni, O.G. Abatan, A. Busari, O. Olayemi Odunlami, C. Nweke, Production and characterization of activated carbon from pineapple waste for treatment of kitchen wastewater, Desalination Water Treat. 183 (2020) 413–424.
[21] P. Ranjan, J. Balakrishnan, A.D. Thakur, Dye adsorption behavior of graphene oxide, Mater. Today Proc. 11 (2019) 833–836.
[22] S.E. Sanni, P. Olowoyeye, E.E. Okoro, B.A. Oni, A.I. Tijani, O. Adegbite, Heterogeneous catalytic conversion of 4-chlorophenol via atomic hydrogen

substitution induced by size-controlled polydisperse nanocobalt, Chem. Eng. Sci. 247 (2022) 117018.
[23] N. Tian, Q. Jia, H. Su, Y. Zhi, A. Ma, J. Wu, S. Shan, The synthesis of mesostructured NH2-MIL-101(Cr) and kinetic and thermodynamic study in tetracycline aqueous solutions, J. Porous Mater. 23 (5) (2016) 1269–1278, https://doi.org/10.1007/s10934-016-0186-z.
[24] M. Tong, D. Liu, Q. Yang, S. Devautour-Vinot, G. Maurin, C. Zhong, Influence of framework metal ions on the dye capture behavior of MIL-100 (Fe, Cr) MOF type solids, J. Mater. Chem. 1 (30) (2013) 8534–8537, https://doi.org/10.1039/c3ta11807j.
[25] T.A. Vu, G.H. Le, C.D. Dao, L.Q. Dang, K.T. Nguyen, Q.K. Nguyen, P.T. Dang, H.T.K. Tran, Q.T. Duong, T.V. Nguyen, G.D. Lee, Arsenic removal from aqueous solutions by adsorption using novel MIL-53(Fe) as a highly efficient adsorbent, RSC Adv. 5 (7) (2015) 5261–5268, https://doi.org/10.1039/c4ra12326c.
[26] W. Wang, J. Wang, S. Zhang, P. Cui, C. Wang, Z. Wang, A novel Schiff base network-1 nanocomposite coated fiber for solid-phase microextraction of phenols from honey samples, Talanta 161 (2016) 22–30, https://doi.org/10.1016/j. talanta.2016.08.009.
[27] J.Y. Wang, Y.C. Li, Y. Xie, K.R. Zhu, A. Alsaedi, T. Hayat, C.L. Chen, Construction of novel graphene-based materials GO@SiO2@C@Ni for Cr(VI) removal from aqueous solution, J. Colloid Interface Sci. 557 (2019) 254–269.
[28] P.M. Wang, L.X. Sun, J.H. Ye, Q. Liu, Z.Y. Fei, X. Chen, Z.X. Zhang, J.H. Tang, M.F. Cui, X. Qiao, Construction of crystal defect sites in UiO-66 for adsorption of dimethyl phthalate and phthalic acid, Microporous Mesoporous Mater. 312 (2021), https://doi.org/10.1016/j.micromeso.2020.110778.
[29] Q. Wen, Y. Wang, Z. Zequan Zeng, F. Qi, P. Gao, Z. Huang, Covalent organic frameworks-derived hierarchically porous N-doped carbon for 2,4-dichlorophenol degradation by activated persulfate: the dual role of graphitic N, J. Hazard. Mater. 426 (128065) (2021), 128065, https://doi.org/10.1016/j.jhazmat.2021.128065.
[30] Z.-h. Yang, J. Cao, Y.-p. Chen, X. Li, W.-p. Xiong, Y.-y. Zhou, C.-y. Zhou, R. Xu, Y.-r. Zhang, Mn-doped zirconium metal-organic framework as an effective adsorbent for removal of tetracycline and Cr(VI) from aqueous solution, Microporous Mesoporous Mater. 277 (2019) 277–285, https://doi.org/10.1016/j.micromeso.2018.11.014.
[31] H. Yan, WuH, K. Li, Y.W. Wang, X. Tao, H. Yang, A. Li, R.S. Cheng, Influence of the surface structure of graphene oxide on the adsorption of aromatic organic compounds from water, ACS Appl. Mater. Interfaces 7 (12) (2015) 6690–6697, https://doi.org/10.1021/acsami. 5b00053.
[32] P. Zhang, J.-L. Gong, G.-M. Zeng, C.-H. Deng, H.-C. Yang, H.-Y. Liu, S.-Y. Huan, Cross-linking to prepare composite graphene oxide-framework membranes with highflux for dyes and heavy metal ions removal, Chem. Eng. J. 322 (2017) 657–666.
[33] L. Zhang, L.L. Wang, Le, L. Gong, X.F. Feng, M.B. Luo, F. Luo, F, Coumarin-modified microporous-mesoporous Zn-MOF-74 showing ultra-high uptake capacity and photo-switched storage/release of UVI ions, J. Hazard Mater. 311 (2016) 30–36.
[34] C. Zhou, E. Almatrafi, X. Tang, B. Shao, W. Xia, B. Song, W. Xiong, W. Wang, H. Guo, S. Chen, G. Zeng, Investigation on the structure-performance of phthalic acid carboxyl position and carbon nitride towards efficient photocatalytic degradation of organic pollutants, Separ. Purif. Technol. 286 (2022) 120464.